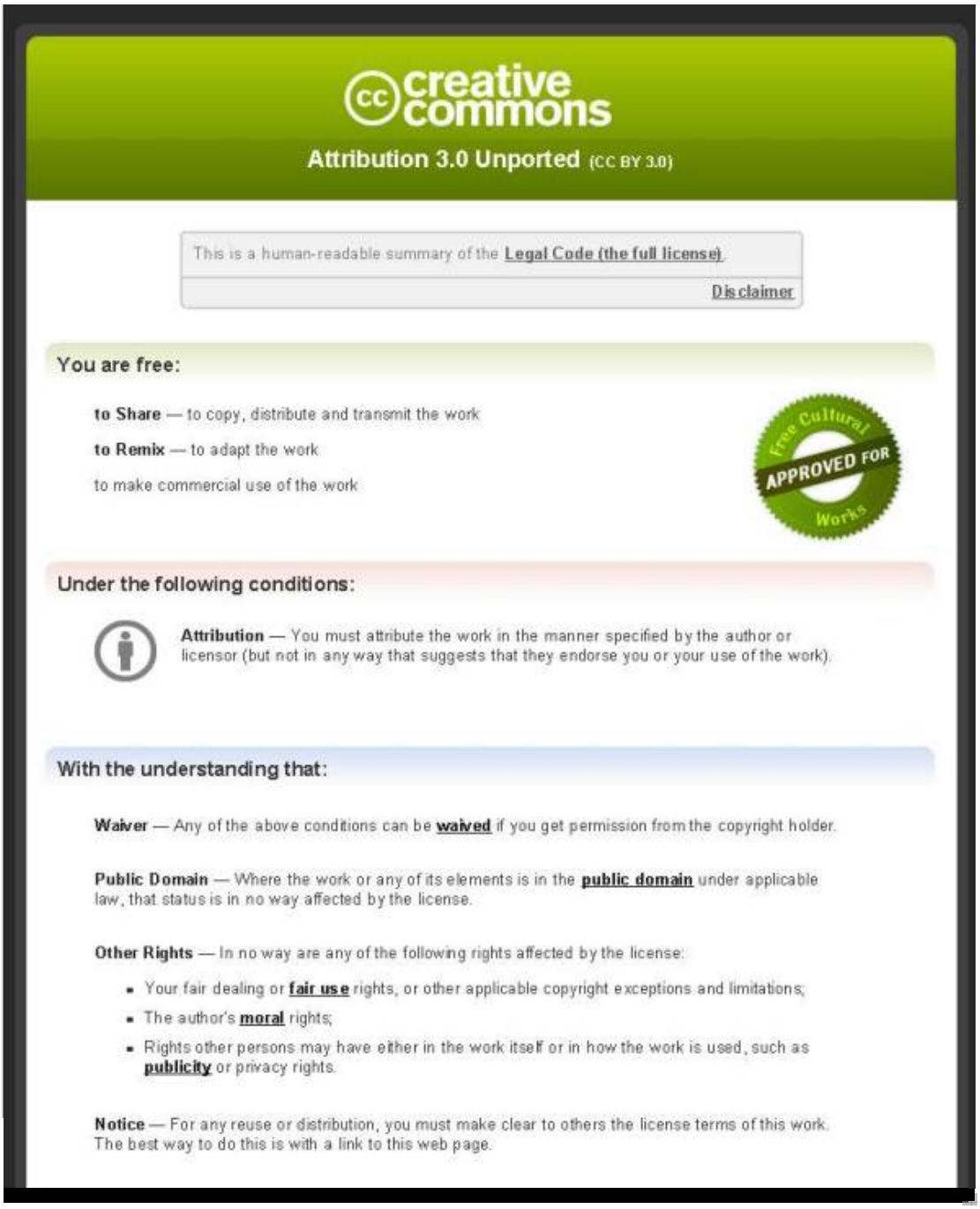

Engineering Structures 56 (2013) 1945–1956

Contents lists available at ScienceDirect

Engineering Structures

journal homepage: www.elsevier.com/locate/engstruct

Design methodologies for one way spanning eccentrically loaded minimally or centrally reinforced pre-cast RC panels ☆

Gary P. Robinson [a,b,*], Alessandro Palmeri [c], Simon A. Austin [c]

[a] Centre for Innovative and Collaborative Engineering, Loughborough University, Loughborough LE11 3TU, UK
[b] Hanson Structherm, Bent Ley Road, Meltham, Huddersfield HD9 4AP, UK
[c] School of Civil and Building Engineering, Loughborough University, Loughborough LE11 3TU, UK

ARTICLE INFO

Article history:
Received 21 November 2011
Revised 18 June 2013
Accepted 30 July 2013
Available online 19 September 2013

Keywords:
Pre-cast concrete
Buckling
Design Assisted by Testing (DAT)
Lumped plasticity
Fibre-hinge model

ABSTRACT

This paper examines and evaluates design methodologies applicable to pre-cast reinforced concrete (RC) panels subjected to eccentric axial load. Theoretical capacities derived from existing regulatory guidance are compared against those determined from experimental investigations, showing that slender RC walls have load capacities significantly higher than the estimates based on current design equations.

A simple computational procedure incorporating lumped plasticity is presented and experimentally validated. It is shown that by utilising a non-linear hinge at the critical cross section, it is possible to effectively simulate the buckling response of the slender walls considered with a modest computational effort. The proposed design strategy emerges as a viable alternative to traditional methodologies by being able to capture the main effects of geometrical and material nonlinearities. It is therefore suggested that this approach, used in conjunction with a probabilistic, semi-empirical design procedure, will lead to design capacities more representative of actual experimental findings.

1. Introduction

Reinforced concrete (RC) panels serve as key structural members for many common building forms. Within pre-cast 'tilt-up' or 'cross-wall' construction typologies for example, such panels provide the fundamental vertical load-carrying system. As a result, many codes of practice devote specific sections to the design and detailing of these elements. The American ACI 318-05 [1], Australian AS 3600-09 [2] and European EC2 [3] design codes all allow using simplified and empirically (or semi-empirically) derived equations [4]. However, because of their inherent simplicity, such equations cannot correctly account for the material and geometric non-linearity in the buckling failure of slender RC elements under eccentrically applied loads [5]. Therefore, large safety factors are adopted, and numerous studies have subsequently demonstrated that these equations significantly underestimate panel capacities when compared to those achieved by experimentation [6,7].

A possible alternative design methodology, also enabled within all of the structural design codes referenced, is to consider the RC panel element as an 'equivalent column', with the appropriate axial-moment interaction equations. However, minimum reinforcement requirements are frequently adopted for pre-cast concrete elements within cross-wall construction, and this steel is also often centrally placed for factors associated with manufacture and durability. Previous studies [8,9] have suggested though, that because the resulting structural response and failure mode of such elements is fundamentally different to those experienced by more heavily reinforced panels, the applicability of the equivalent column method in such instances is questionable.

In order to provide a way to design non-standard structural components and/or to overcome the limitations of existing design rules, the Eurocodes (through specific provisions within EC0 [10]) enable an alternative strategy based on a combination of testing and calculation. This Design Assisted by Testing (DAT) procedure exploits probabilistic considerations to ensure that appropriate factors of safety are applied to predictions of structural capacity. These factors can be directly determined from experimental work conducted as long as the number of tests available is sufficient for a meaningful statistical interpretation [11]. In the case of slender RC panels with minimum/central reinforcement, however, recent research [12] has found that, because a large and systematic conservatism exists between experimentally observed capacities and the current design procedures, these methods cannot provide

* Corresponding author at: Centre for Innovative and Collaborative Engineering, Loughborough University, Loughborough LE11 3TU, UK. Tel.: +44 (0)1484 850098; fax: +44 (0)1484 851388.

E-mail addresses: G.P.Robinson@lboro.ac.uk (G.P. Robinson), A.Palmeri@lboro.ac.uk, Dynamics.Structures@gmail.com (A. Palmeri), S.A.Austin@lboro.ac.uk (S.A. Austin).

0141-0296/$ - see front matter © 2013 The Authors. Published by Elsevier Ltd. All rights reserved.
http://dx.doi.org/10.1016/j.engstruct.2013.07.041

Nomenclature

A_c	gross sectional area of concrete panel
A_s	cross-sectional area of steel in the panel section
b	least-squares parameter accounting for variables omitted in theoretical mechanical model
d_b	effective depth of longitudinal reinforcing steel
D_n	difference between theoretical and empirical cumulative distribution to Kolmogorov test
e	eccentricity of the load measured at right angles to plane of the wall
e_{tot}	eccentricity of the load at critical panel section
e'	$e-(t/6)+(M_{CR}/P_E)$ = equivalent eccentricity parameter
E_c	modulus of elasticity of concrete
f_c	compressive cylinder strength of concrete
f_{ct}	flexural cracking strength of concrete
f_y	yield strength of steel
$g_{rt}(\mathbf{X})=r_t$	deterministic value of the theoretical resistance function
F_c	resultant force from concrete rectangular stress block
F_{NH}	notional horizontal point load applied to account for geometric imperfections
F_Δ	ideal cumulative distribution function
H	effective height of the wall
I	second moment of area of concrete cross section
$k_{d,n}$	design fractile factor
L	effective length of panel
L_P	length of analytical fibre hinge (i.e. length along which final hinge failure occurs)
L_S	the shear span of the member
M	bending moment at critical panel section due to load eccentricity
M_0	nominal out-of-plane member moment capacity
M_{CR}	flexural cracking moment of the wall section without any axial force
N	externally applied axial force
N_U	ultimate design axial strength of a wall in compression
P_E	Euler buckling load
r_{ei}	experimental capacity for the ith test
r_{ti}	theoretical resistance determined using the measured parameters X for specimen i
r_d	resulting design resistance function
t	thickness of the wall
T_0	age of concrete at time of loading
$V_\Delta=\sigma_\Delta/\mu_\Delta$,	coefficient of variation for error terms
V_X	coefficient of variation of X
V_R	coefficient of variation in element resistance
X	array of j basic variables $X_1 \ldots X_j$
δ'	lateral deflection at critical section of wall panel
δ	model error
$\Delta=\ln(\delta)$	logarithm of the error term
ε_c	strain at extreme compressive fibre
ε_{co}	ultimate compressive strain of concrete
$\varepsilon_{(c,\infty)}$	long term deformation of concrete element due to creep at the infinite time $T=\infty$
Φ_Δ	empirically derived cumulative distribution function
$\theta=\arctan(b)$	the angle that the least squares regression line forms with horizontal axis
θ_1	rotation (relative to the vertical axis) at the pinned joint of the simple panel element
κ	curvature at critical section of wall panel subject to eccentric loading
$\lambda=H/t$	panel element slenderness
μ	mean of n sample results
$\nu=1+0.4\times10^{-3}f_c$	dimensionless shape parameter for the concrete material model
ρ	reinforcement ratio within reinforced concrete panel
φ	strength reduction factor
σ_c	stress in concrete element
σ_δ	standard deviation of the model error
$\phi_{(\infty,T_0)}$	creep cofficient at time $T=\infty$
ψ	angle between simplified deflected shape and vertical at simple support
$\psi_i=1/200$;	rads, imposed angle of rotation to allow for geometric imperfections
$\omega=\kappa L_p$	rotation of fibre hinge at critical panel location

a suitable design, or 'resistance' function for the DAT procedure. Consequently, an alternative theoretical model, which more appropriately reflects actual buckling capacity, is required.

In this paper, the use of a 'lumped plasticity' model is proposed in order to achieve a truer representation of the system's non-linearity, and therefore deliver more accurate predictions of the failure capacity of the wall elements. By using a non-linear 'fibre-hinge' element at the known location of maximum moment, the entire inelasticity of the element can be concentrated at this location. It is shown that because this computational method accounts for non-linear material and geometric effects, it is in fact more effective in simulating the buckling response of the slender walls relative to the existing design methods. This has been validated (and the resulting improvement quantified) by comparing the predictions of panel capacity against actual experimental data (partly collected through full-scale tests carried out as part of this study and partly using those available within existing literature). Given the improved agreement with the empirical evidences, the paper demonstrates the suitability of adopting such a design procedure for the problem in hand, also presenting the resulting design curve and providing conclusions regarding its application in practice.

2. Current design methods

The aim of this section is to briefly review the design procedures suggested in the existing regulatory guidance, which in turn will allow (in the second part of the paper) the quantification of the improved effectiveness of the proposed design strategy for slender, centrally reinforced precast concrete panels.

2.1. Simplified design capacity expressions

In order to enable direct comparison between the American (ACI 318-05), Australian (AS 3600-09) and European (EC2) building codes, the relevant design expressions have been rearranged, as part of Table 1, in the form of the dimensionless design axial strength ratio [6,7,12]. In these expressions, $F_c=f_cA_c$ is the compressive force within the stress block, and N_U is the ultimate value of the axial force applied with eccentricity $e=t/6$.

The design capacities from each of the specified equations are plotted in Fig. 1 as a function of the slenderness ratio $\lambda=H/t$. It is apparent that the European code (thick solid line) deals with the slenderness of axially loaded members in a manner different

Table 1
Design expressions for simply one-way spanning RC panels to the major international codes ($e = t/6$; $\phi = 0.6$ or 0.7).

Building code	Design expression
ACI 318-05 [1]	$\frac{\phi N_u}{F_c} = 0.385\left[1 - \frac{\lambda^2}{1024}\right]$
AS 3600-01 [2]	$\frac{\phi N_u}{F_c} = 0.288\left[1 - \frac{\lambda^2}{1000}\right]$
EN 1992-1-1 [3]	$\frac{N_u}{F_c} = 0.57[0.76 - 0.026\lambda] \leqslant 0.83 - \frac{\lambda}{400}$

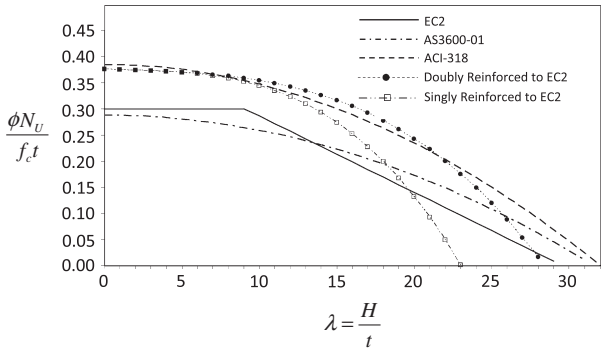

Fig. 1. Normalised panel capacity design curves according to simplified design equations of international codes ($e = t/6$; $\phi = 0.6$ or 0.7) and the 'equivalent column' methodology in EC2 ($\rho = A_s/Lt < 0.3\%$).

to the American (dashed line) and Australian (dot-dashed line) codes, which incorporate parabolic expressions to account for the curvature of the section and the modified line of action of the eccentric load. In contrast, EC2 accounts for the secondary moments by applying a concentrated, notional, horizontal load (F_{NH}) at the point of maximum moment in the panel. In this way, the European code adopts a triangular curvature distribution, which leads to a second linear (rather than parabolic) term, and reduces significantly the design capacities for slender elements.

For comparison purposes, Fig. 1 also shows the design capacities for both doubly (filled circles) and centrally reinforced (empty squares) panel elements using the equivalent column methodology. Specifically the method of 'Nominal Curvature' is utilised as suggested by the European code (more details are provided in Section 2.3), adopting the minimum reinforcement ratio specified, such that:

$$\rho = \frac{A_s/L}{t} \leqslant 0.3\%, \tag{1}$$

in which A_s/L is the cross-sectional area of reinforcement per unit length of the panel.

What Fig. 1 reveals is that by adopting the equivalent column design methodology for doubly, yet minimally reinforced, panel elements one can obtain enhanced capacities for structural elements up to a slenderness of $\lambda \leqslant 27$. However, a much steeper falling branch is seen for centrally reinforced panel elements, due to the small effective depth of the reinforcement within the panel.

2.2. Limitations of existing simplified design equations

The current, code-compliant, simplified equations allow no account to be taken of either the quantity or distribution of longitudinal reinforcement, nor modifications of the concrete stress block if needed (e.g. for non-standard concretes such as, steel fibre reinforced or alternative sustainable concrete mixes). Moreover, these methods cannot account for the inherent non-linearity associated with the buckling failure of slender RC panels, or design situations where the axial load may be applied outside the section's middle third.

Further, as can be seen from Fig. 1, the major international design codes currently restrict slenderness ratios of RC panels to $\lambda < 30$ despite numerous studies having presented and demonstrated the applicability of design equations associated with the capacity of very slender ($30 \leqslant \lambda \leqslant 50$) one way spanning RC panels [13].

2.3. Suitability of equivalent column design

Prima facie, the equivalent column methodology would seem to address the main limitations identified above, by allowing consideration of material non-linearity and strain compatibility. However, in the case of the minimally or centrally reinforced panels, contemporary research [12,14,15] challenges the applicability of this design procedure.

The failure of an equivalent column is considered to occur when the moment induced at the critical section of the panel element exceeds the 'flexural capacity' of the element at this location. Kripanarayanan [14] however, has demonstrated that reinforcement amounts of $\rho = 0.75$–1.0% are needed for the reinforcement to affect the failure loads of slender walls. Subsequent test data, investigating singly reinforced RC panels adopting reinforcement ratios up to 3% [15] have also shown that the effect of increasing the amount of centrally placed reinforcement on the panel's capacity is negligible, even above the $\rho = 1\%$ level determined for doubly reinforced panels.

What these findings prove is that the structural performance of such panels depends mainly on the 'flexural cracking' response of the element, i.e. when the concrete section at the critical location cracks in flexure the resulting concentrated loss of stiffness, combined with the lack of influential tension steel, controls the ultimate stability of the panel much more than would occur with doubly reinforced panels where $\rho \geqslant 1\%$. As a consequence, the ultimate axial capacity of the RC wall element becomes dependent on the post-cracked flexural stiffness of the cross-section, and appropriate account must be taken of the contribution of the concrete acting within both the tension and compression zone. It follows that the code-compliant equivalent column procedure should not be used for the design of centrally and/or minimally reinforced panels, as their resulting axial capacity would primarily depend on the stiffness of the un-cracked panel section and the tensile strength of the concrete in flexure. Further, a moment magnifier should also be applied, depending on the ratio of applied axial load to the theoretical buckling resistance of the panel, in a manner identical to that considered by Sanjayan [16]. He proposed to evaluate the axial load capacity N_U of a slender RC wall as:

$$N_U = \frac{1}{e'}(M_{CR} - M_0), \tag{2}$$

where $e' = e - (t/6) + (M_{CR}/P_E)$ provides an equivalent eccentricity in order to account for the variation in panel's flexural stiffness up to and post cracking, while $M_{CR} = f_{ct}Lt^2/6$ is the flexural moment required to cause the panel to crack.

The important question arising from Eq. (2) is whether it is in fact the flexural strength of the concrete acting within the tension zone of the RC panel that dominates the resulting capacity of the panel; or is it instead the true response of the concrete's compression block. In this regard, a certain degree of disagreement has been identified within existing literature ([8,9]).

3. Design Assisted by Testing (DAT)

The evidence thus far presented allows us to conclude that current, commonly adopted design procedures for the load capacity of

centrally and/or minimally reinforced concrete walls appear over-conservative, restrictive and limited in regards to their design application. However, the European code [3] offers a potential alternative design procedure based on a combination of testing and calculation. This design methodology, which has been explored in recent studies [17,18], potentially allows experimental data to be utilised to enable a more realistic code-compliant estimation of the ultimate axial capacity of slender RC panels.

In an attempt to assess the applicability of this Design Assisted by Testing (DAT) method to the problem under consideration, a programme of experimental investigation was conducted.

3.1. Test panels and experimental setup

Sixteen $L = 500$ mm wide and $t = 100$ mm thick pre-cast concrete panels of varying height and slenderness (λ between 25 and 30), were axially loaded, with a range of eccentricities also adopted to reflect common construction and design cases. Table 2 provides a summary of the test samples prepared, with an overview of the experimental arrangement utilised also illustrated within Fig. 2. The testing rig had a capacity of 4000 kN with the loading beam designed to ensure the transmission of a uniformly distributed load across the top of each panel at eccentricities of 0, 5 mm (t/20), 17 mm (t/6) and 33 mm (t/3). The top and bottom hinged support condition, illustrated within Fig. 2(c), was simulated by placing a 25 mm high-strength steel rod on a 50 mm thick steel bearing plate. Displacement transducers recorded out-of-plane displacements (δ') at the centre of the panel and strain readings, with respect to the tension face of the buckling panel, were also taken with a digital portal gauge at the known critical section (Fig. 2(b)).

Because another experimental objective was to assess the sensitivity of a panel's buckling capacity to the element becoming cracked at its critical section, six of the panels were axially loaded in a pre-cracked condition, with the fissure induced in flexure, prior to loading.

3.2. Experimental findings and use in DAT

Table 2 summarises the load capacities obtained for each of the tests undertaken. As can be seen, the ultimate capacity of the panels (sixth column) far exceeded the predictions of both simplified code equations (seventh column) and equivalent column methodology (eighth column) as enabled within EC2. This is not surprising, as Fig. 1 shows that for a panel slenderness of $\lambda = 30$ all the commonly adopted methodologies would predict a load carrying capacity approaching (or equal to) zero.

Our experimental findings thus support past research, and confirm that simplified design equations provide overly conservative estimates of slender RC panel capacity. More importantly, this testing campaign also demonstrates that the axial capacity of centrally reinforced elements is effectively independent of the flexural tensile strength of the concrete, as similar capacities have been experimentally observed for panels in the cracked (C) or un-cracked (U) initial condition. This is one of the key findings of this testing, as it allows us to conclude that the contribution due to the concrete's post-cracked behaviour (specifically the response of the compressive stress block) is crucial in determining the element's capacity. The observed failure typology also supports this finding, with a

Table 2
Experimentally observed and predicted failure capacities.

Panel no.	Slenderness (λ)	f'_c (N/mm^2)	e (mm)	C (Cracked) or U (Un-cracked)	N_u (kN)			
					Test	EC2 Simp Eq	EC2 Eqv Col	Proposed
1	30	52.2	0	C	781	0	0	737.5
2	30	52.2	0	C	762	0	0	737.5
3	30	53.2	5	C	672	0	0	675
4	30	53.2	5	C	725	0	0	675
5	30	49.1	17	C	595	0	0	517
6	30	49.1	17	C	557	0	0	517
7	25	51.5	17	U	871	24.35	0	803
8	25	51.5	17	U	858	23.93	0	803
9	28	52.4	17	U	692	6.96	0	643
10	28	52.4	17	U	683	7.07	0	643
11	30	51.6	17	U	582	0	0	531
12	30	51.6	17	U	597	0	0	531
13	30	51.6	17	U	572	0	0	531
14	30	51.6	17	U	568	0	0	531
15	30	52.4	33	U	322	0	0	302
16	30	52.4	33	U	336	0	0	302

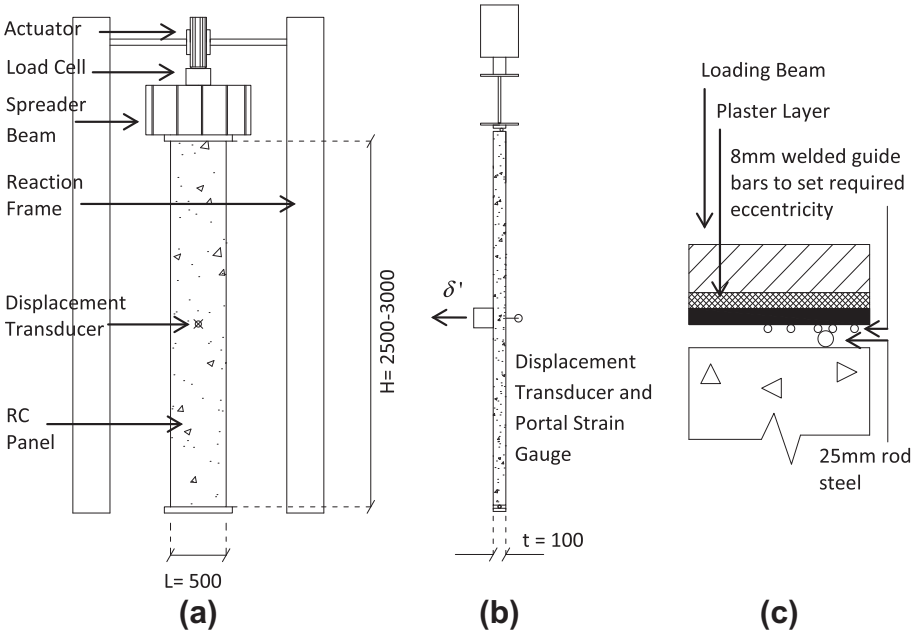

Fig. 2. Experimental set-up: Test rig elevation (a); test rig section (b); and pin joint loading detail (c). All dims in mm unless noted.

Fig. 3. Brittle failure observed in both pre-cracked and un-cracked RC panel elements.

compressive spalling (Fig. 3(a)) observed, along with extensive flexural cracking for both cracked and un-cracked initial conditions (Fig. 3(b)).

Moving from the above considerations, the investigation then examined whether the experimental results obtained from the testing programme could be used to derive a more representative design curve by application of the DAT method. The procedure consists of seven distinct steps [10]:

- Firstly, a suitable theoretical resistance model is required to predict the capacity of the element (step (i)).
- The theoretical model has to be validated against experimental data, through measurements of the relevant variables within the tests (step (ii)).
- Statistical techniques are then used to 'fine-tune' the prediction capability of the theoretical model [17] (step (iii)).
- The definition of a semi-probabilistic capacity curve can then be progressed as long as the residual model error (δ) is correctly quantified and incorporated (step (iv)).
- The design value of the capacity model (Fig. 11) is consequentially obtainable (step vi) following the estimation of its mean and variance (step v), based upon the assumption of a normal or log-normal distribution, the validity of which has to be checked (step vii).

3.3. Theoretical resistance model for the DAT procedure

The DAT procedure method, as detailed above, relies on the availability of a satisfactory theoretical capacity model able to represent the most significant aspects of the structural behaviour relating to the component under consideration (step (i)). The resistance function can be mathematically expressed as:

$$r_t = g_{rt}(\mathbf{X}), \tag{3}$$

where g_{rt} is the theoretical model, which depends on the array X collecting all the basic variables influencing the structural capacity. In the present study, such variables may include the compressive (f_c) and tensile capacities (f_{ct}) of the concrete, the geometrical parameters (λ, L and H) as well as the reinforcement ratio (ρ) and its arrangement. All of these variables were, of course, captured by the experimental programme undertaken (step (ii)). One must also ensure, however that the adopted theoretical resistance function, r_t, provides an acceptable correlation with the experimental resistance data, r_e, so as to be considered suitable for use within the derivation of the sought design capacity (step (iii)). This check can be done by considering the least-squares best fit to the slope b between r_t and r_e, i.e. by minimising the following quadratic expression:

$$S(b) = \sum_{i=1}^{n} (r_{e,i} - b g_{rt}(\mathbf{X}_i))^2, \tag{4}$$

where $r_{e,i}$ and $r_{t,i} = g_{rt}(\mathbf{X}_i)$ constitute the ith pair of an experimental value and theoretical prediction. The condition $dS/db = 0$ allows computing the optimal value of the angular coefficient b:

$$b = \frac{\sum_{i=1}^{n} r_{e,i} r_{t,i}}{\sum_{i=1}^{n} r_{t,i}^2} = \tan(\theta), \tag{5}$$

$\theta = \arctan(b)$ being the angle that the regression line forms with the horizontal axis (Fig. 4).

In a first stage, we considered the case in which the theoretical model of Eq. (3) is provided by the empirical design equation (Table 1, last row) and the equivalent column method (Eq. (2)) within EC2. Fig. 4(a) and (b) illustrate that such procedures provide a poor correlation when compared to our experimental results, as well as other published test capacities [9,13,15]. Indeed, both theoretical models result in a least-squares best fit which is significantly divergent from the recommended of $\theta = \pi/4 \cong 0.785$ (i.e. one-to-one slope), being $\theta = 1.23$ for the simplified/empirical design equation (dashed line, top-left graph) and $\theta = 1.15$ for the equivalent column design (dot-dashed line, top-right graph). It can also be seen that the discrepancy of results can be greater than 40%, which has been suggested as an acceptable limit within the technical literature [17].

4. Computational method and experimental verification

4.1. Lumped plasticity modelling

The results presented in the previous section highlight the need for a new and more efficient design procedure (for inclusion as part of step (i)) if minimally and/or centrally reinforced panels are to be designed using the DAT method.

One such potential procedure has been devised as part of this study through the application of the lumped plasticity idealisation. This is a widely adopted model, particularly utilised in earthquake engineering and robustness assessment, to determine the ultimate performance of a structural system by increasing step by step the load multiplier until failure (push-over or push-down analysis). For the structural problem in hand, the entire inelasticity of the element has been concentrated at a single position by the use of a non-linear fibre 'hinge', since the location of maximum moment (and thus the critical section for the span) is known (see Fig. 5(a)).

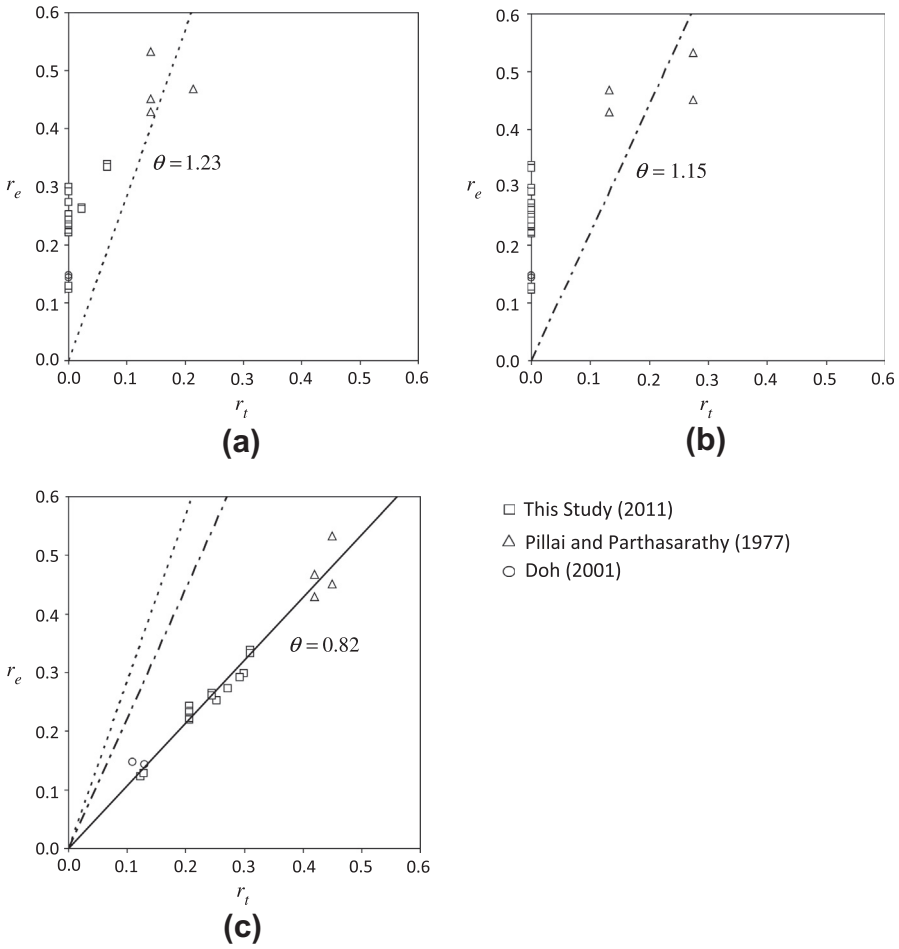

Fig. 4. Comparison between theoretical and experimental results: Simplified design equation to EC2 (a); equivalent column design method to EC2 (b); and alternative computational design approach (c).

In this representation, the element's cross-section is subdivided into a number of elementary layers or fibres [19], to which the appropriate material properties are then assigned (see Fig. 5(b)). The non-linear moment–curvature relationship of the fibre hinge can then be determined for a range of axial loads assuming plane cross sections. Fig. 5(d) illustrates the moment-rotation behaviour computed for an un-cracked panel section loaded at an eccentricity of $e = t/6$, while Fig. 5(c) shows a typical distribution of the compressive stress σ along the panel's depth at the critical location.

In the proposed computational model, the rotation ω experienced by the fibre hinge is evaluated under the assumption of a uniform curvature κ over the adopted length L_p of the plastic element, i.e. $\omega = \kappa \cdot L_p$. In this study, because of the mesh reinforcement layouts commonly detailed for minimally as well as centrally reinforced panels (Fig. 5(b)), the length of the plastic hinge and the material model were selected to reflect the lack of ductility observed experimentally for the unconfined concrete at the critical cross section [20,21]. Accordingly, the hinge lengths adopted were computed from the expression proposed (and experimentally validated) by Panagiotakos and Fardis [22] for unconfined RC panels and column elements subjected to monotonic loading:

$$L_P = 0.18L_S + 0.021d_b f_y, \tag{6}$$

where $L_S = H/2$ is the shear span of the member, $d_b = t/2$ (for the panels considered as part of this study) is the effective depth of the longitudinal reinforcement and f_y is the yield strength of that reinforcement.

For validation purposes, simple equilibrium equations are used within Appendix A to check the results of the numerical analysis.

4.2. Experimental validation of the computational model

As can be seen from Table 2, the ultimate load capacities predicted by the proposed computational method with lumped plasticity (last column) compare very well to those experimentally observed (sixth column), with the method also seen to consistently slightly underestimate the actual panel buckling capacity within a range of 3–13%.

In our analyses, the three-parameter concrete material model initially proposed by Mander et al. [23] and illustrated within Fig. 6(a) was adopted for the stress–strain constitutive law $\sigma_c(\varepsilon_c)$ of the unconfined concrete, where

$$\sigma_c = f_c \frac{v\left(\frac{\varepsilon_c}{\varepsilon_{co}}\right)}{(v-1)+\left(\frac{\varepsilon_c}{\varepsilon_{co}}\right)^v}, \tag{6a}$$

where $v > 1$ is a dimensionless shape parameter to be evaluated through the empirical relationship [24,25]:

$$v = 1 + 0.4 \times 10^{-3} f_c. \tag{6b}$$

Importantly, the concrete material model can be easily modified if the performance of other concrete types, such as high-strength concrete and fibre reinforced mixes, has to be accounted for.

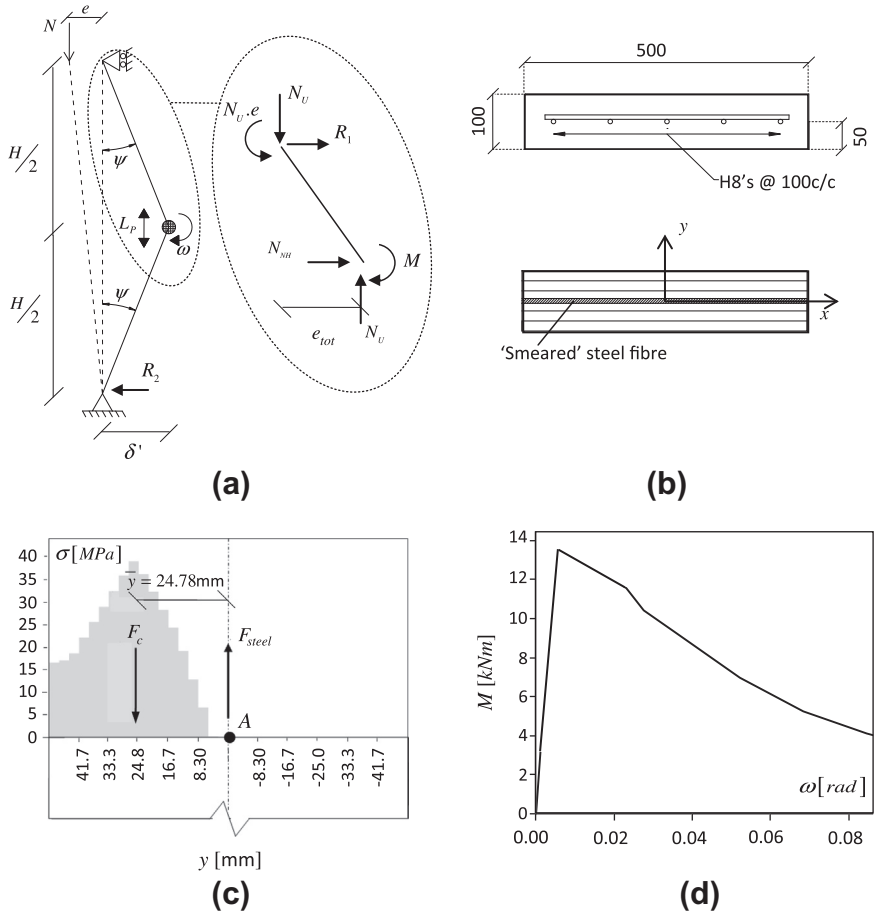

Fig. 5. Key aspects of the lumped plasticity analysis: Computational idealisation of experimental set-up (a); reinforcement layout and fibre hinge idealisation of wall panel cross section (b); resulting compressive stress block (c); and resulting moment rotation response of fibre hinge (d). All dims in mm unless noted.

Because a displacement-controlled non-linear push-down analysis is adopted, it is possible to assess the resulting deformations and strains induced within the fibre hinge incrementally up until (and also beyond) the ultimate failure load. These numerical outputs in terms of deflection and strain, relating to the 'tensile' face of the buckling panel (Fig. 2(b)), have been plotted (thick lines) against the actual experimental data (symbols) in order to investigate whether the adopted computational strategy accurately captures the true structural behaviour of the RC wall elements. The computationally predicted behaviour appears to closely represent that observed within testing, although the lumped plasticity computational model tends to underestimate the deformation of the element at failure (Figs. 7 and 8). The almost linear elastic nature of the load–strain plots also correctly captures the relatively brittle failure mechanism observed (Fig. 3).

4.3. Sensitivity analyses

The sensitivity of the proposed method to variations in the constitutive law (see Eqs. (7) and (8)) adopted for the unconfined concrete was also investigated. Specifically, the study focussed on the effect of the softening branch and long-term deformations.

In a first stage, two alternative representations of the stress–strain relationship for unconfined concrete, illustrated within Fig. 6(b) and (c), were adopted to re-analyse the wall panels. The behaviour illustrated within Fig. 6(b) is based on the modified Kent–Park [24] model proposed by Scott et al. [25], in which pre-peak and post-peak behaviour are given by:

$$\sigma_c = Kf_c \times \begin{cases} \frac{2\varepsilon_c}{0.002K} - \left(\frac{\varepsilon_c}{0.002K}\right)^2, & \varepsilon_c \leqslant 0.002K; \\ 1 - Z_m(\varepsilon_c - 0.002K), & \varepsilon_c \geqslant 0.002K, \end{cases} \tag{7}$$

where $K = 1$ for the unconfined case under consideration, and the dimensionless parameter Z_m controlling the post-peak slope can be evaluated as:

$$Z_m = \frac{0.5}{\frac{3+0.29f_c}{145f_c-1000} - 0.002K} \tag{8}$$

in which the compressive strength of the concrete f_c must be expressed in MPa.

The second alternative considered, illustrated within Fig. 6(c), was to discount the tension-softening branch completely from the adopted Mander's representation of the material behaviour. The predicted panel capacities varied between 2% and 5%, which demonstrates that the proposed fibre-hinge modelling for the centrally reinforced concrete section is largely insensitive to such variations in the unconfined stress–strain model.

A second stage assessed the effects of the creep on the long-term response of the RC wall panel by appropriately modifying the material model adopted for the unconfined concrete. Creep in concrete is a complex phenomenon, which may depend on ambient humidity, size of the element, the mix of constituents, the strength of the material when stressed as well as the magnitude and duration of the applied loads [26]. Despite this inherent complexity, the ultimate creep strain can be effectively computed by factoring the observed elastic strain by a creep coefficient such that:

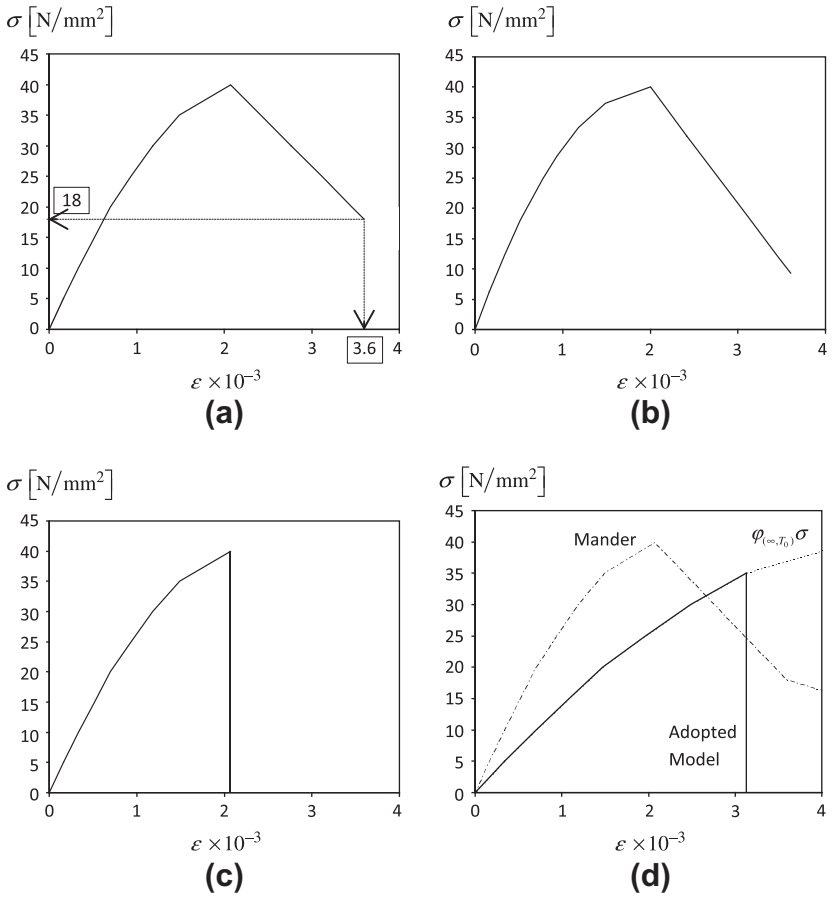

Fig. 6. Material models adopted within computational analysis: Mander [24] (a); Park–Kent [25] (b); Mander with modification to tension softening branch (c); and accounting for time-dependant 'creep' effects (d).

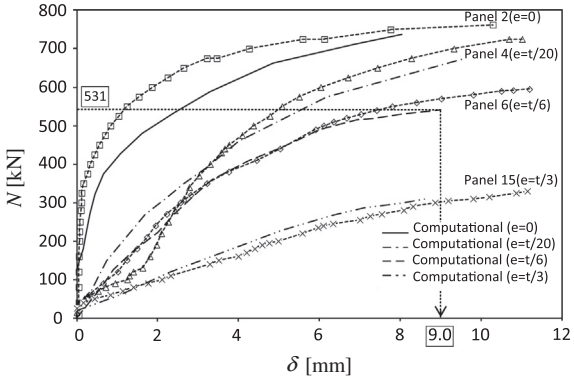

Fig. 7. Experimental and computational load–deflection curves for panels with varying eccentric loads.

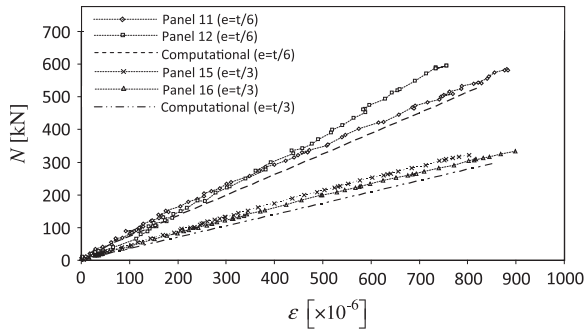

Fig. 8. Experimental and computational strain plots for the outer fibre in tension for panels with varying eccentric loads.

$$\varepsilon_{c,\infty} = \varphi_{(\infty,T_0)}\left(\frac{\sigma_c}{E_c}\right), \tag{9}$$

In our investigations, creep effects were evaluated according to the procedure detailed within EC2, assuming: (i) relative humidity of 50% (consistent with an indoor environment); (ii) class R, rapid strength gain mix design, containing a negligible amount of GGBS (Ground Granulated Blast Slag), for the C40/50 concrete utilised for the test panels; (iii) thickness of the walls $t = 100$ mm; and (iv) age of the concrete when loaded $T_0 = 28$ days. The creep coefficient so computed is $\varphi_{(\infty,T_0)} = 2.1$, which is in line with observed strains stated within literary guidance [27]. Fig. 6(d) shows the modified constitutive law for the unconfined concrete, in which for the same value of the stress σ_c, the strain $\varepsilon_c = \varepsilon_{c,\infty}$ has been increased by the creep coefficient. However, the original value for acceptable strain deformation has been maintained, and this results in the failure of the panel occurring within the rising linear branch of the stress–strain relationship. By allowing for the effects of creep in this way, a reduction in the predicted panel capacities of 20% is observed. Because of the significance of these time-dependent affects, the proposed modified-material model should be adopted within the lumped plasticity representation (or a further factor should be applied retrospectively to the panel capacities derived) before the method is used in the determination of actual design predictions.

5. Structural capacity via DAT

5.1. Probabilistic model for the structural resistance

It has already been shown (see Table 2) that the proposed lumped-plasticity computationally modelling, with a single fibre hinge at the critical mid-span location, is able to capture effectively the buckling failure of slender RC panels, much more than the existing design procedures. To quantify the improved correlation between experimental data, $r_{e,i}$, and theoretical prediction, $r_{t,i} = g(X_i)$, Eq. (5) was used to evaluate the angular coefficient b of the regression line for the proposed approach (see step (iii) of the procedure, as summarised in Section 3.2). A value $b = 1.07$ was found using the whole set of $n = 22$ data points (16 points from our experimental work, shown in Table 2, and six points from previously published studies). The corresponding angle with the horizontal axis is $\theta = \arctan(b) = 0.82$ (see Fig. 4(c)), which has a much better fit to the ideal value ($\theta = 0.785$) compared to the correlation achieved with the EC2 empirical design equation (Fig. 4(a)) or equivalent column methodology (Fig. 4(b)). The condition $b > 1$ confirms that the proposed computational model is conservative (i.e. the theoretical resistances tend, on average, to be slightly less than the corresponding experimental capacities).

However, the fact that the resulting least-squares best fit does not equal the $\pi/4 = 0.785$ ideal means that the proposed theoretical function does not provide an exact and complete representation of the failure mechanism of the structural members under investigation. Within the DAT context, therefore, the angular coefficient b can be interpreted as a statistically-based correction parameter which fine-tunes the theoretical predictions to match, on average, the experimental data. This correction, whose effectiveness increases with the number of data points, eliminates the systematic sources of inaccuracy, due for instance to secondary phenomena not captured and/or included within the chosen theoretical model. Once the least-squares regression coefficient b has been applied to the theoretical predictions, working now within a probabilistic framework, the residual discrepancy still remaining for the ith data point can be modelled as the generic realisation δ_i of a random variable δ with unitary mean value $\bar{\delta} = 1$ and standard deviation σ_δ (step (iv) of the procedure). Therefore, the probabilistic model of the structural resistance becomes:

$$r = b r_t \delta, \tag{10}$$

while the ith sample of the model error δ is given by:

$$\delta_i = \frac{r_{e,i}}{b r_{t,i}}. \tag{11}$$

Either a Gaussian [17] or Log-Normal distribution can be adopted to describe the random variable δ. Theoretically speaking, the latter seems more appropriate, as δ cannot be negative (see Eq. (11)). However, in practice, the Gaussian model could be a viable alternative, particularly if the standard deviation σ_δ is small. The data points relating to the residual errors between the theoretical and experimental values have been used to assess the goodness-of-fit for both potential probabilistic distributions. Fig. 9 compares the empirical Cumulative Distribution Function (CDF) $\Phi_\Delta(\delta)$ obtained from the experimental data points (filled diamonds) with the ideal CDF $F_\Delta(\delta)$ of both Gaussian (solid line) and Log-Normal (dashed line) random variables having the same mean value and standard deviation of the available experiments, that is:

$$\mu_\Delta = \frac{1}{n}\sum_{i=1}^{n}\delta_i = 1.0053; \quad \sigma_\Delta = \sqrt{\frac{1}{n-1}\sum_{i=1}^{n}(\delta_i - \mu_\Delta)^2} = 0.0346. \tag{12}$$

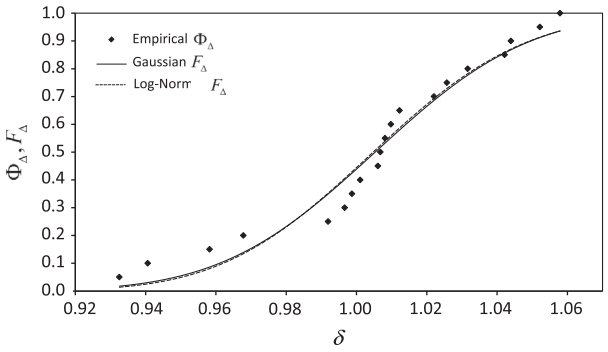

Fig. 9. Statistical check of error properties. Cumulative distribution of the model error (δ).

It can be seen that both theoretical models can be used to describe the model error δ. The one-sample Kolmogorov–Smirnov test [17] was used to confirm the goodness-of-fit for both probabilistic distributions (in line with step (vii) of the DAT procedure, as detailed in Section 6.2) and very similar values of the test statistic for the $n = 22$ data points were obtained, meaning that more samples would therefore be needed in order to select the most appropriate distribution.

An implicit assumption made while introducing Eq. (10) is that the model error δ is independent of the theoretical prediction $r_t = g_{rt}(\mathbf{X})$. Among the j basic design variables collected by the array $\mathbf{X} = \{X_1, X_2, \ldots, X_j\}$, the compressive strength of the concrete, $X_1 = f_c$, and the relative eccentricity of the load, $X_2 = e/t$, are deemed to play the most important roles within our set of data. It is necessary therefore to prove that these quantities are actually uncorrelated to the observed model error. In order to do this, the corresponding scatter plots for the available data points have been reported within Fig. 10, which does not show any significant statistical pattern and therefore confirms our assumption.

This is an important finding, as it means that however the engineer chooses to account for the effects of possible deviations in material properties, geometry of the structural element and position of the load, the resistance function provided by the proposed computational model remains valid.

5.2. Effects of the basic design variables

In order to be applicable in practice, the final resistance function developed through the application of the DAT method must account for any scatter directly associated with the basic design variables identified within Eq. (3), e.g. those relating to material strength. Because of the limited number of tests, our sample may not be fully representative of the behaviour of the population in relation to the basic variables that control the structural response of the element. The DAT method, as formulated within the European code EC0 [10], allows for incorporating such additional sources of uncertainty through the use of a Coefficient of Variation (CoV) $V_{X,i}$ for each of the j basic design variables, whose statistical description must be preliminarily pursued. According to EC0, the CoV of the resistance, V_R, can be estimated by combining the CoVs of all the random/uncertain variables contributing to the structural response, that is:

$$V_R \cong \sqrt{\left(V_\Delta^2 + 1\right)\left[\prod_{i=1}^{j}\left(V_{X,i}^2 + 1\right)\right] - 1}, \tag{13}$$

where $V_\Delta = \sigma_\Delta/\mu_\Delta$ is the CoV of the model error δ. From the expression above, one can demonstrate that the CoV of the theoretical resistance, $V_{R,t}$, is given by:

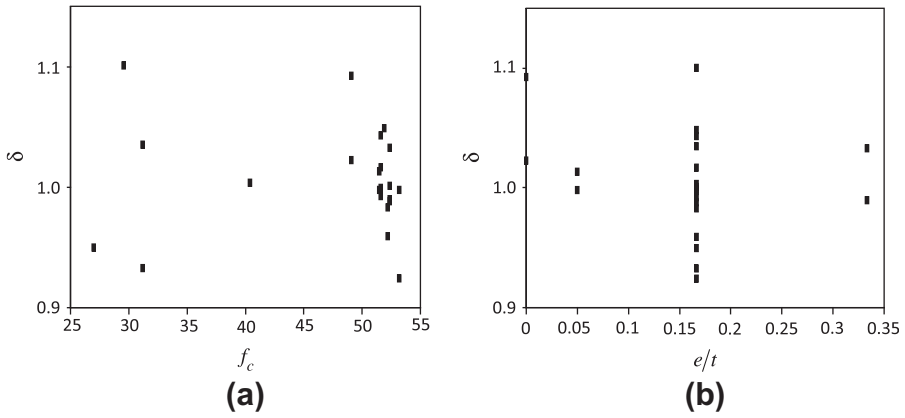

Fig. 10. Scatter diagram of compressive strength (a) and normalised eccentricity (b) versus model error.

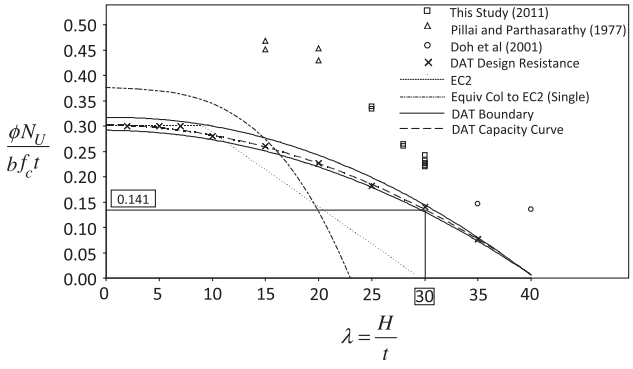

Fig. 11. Alternative panel capacity curve developed from the use of the lumped plasticity idealisation with the DAT procedure ($e = t/6$).

$$V_{R,t} \cong \sqrt{\frac{V_R^2 - V_\Delta^2}{V_\Delta^2 + 1}}, \tag{14}$$

which for moderate level of uncertainty pertaining to the basic design variables within the problem in hand, can be approximated as:

$$V_{R,t} \cong \sqrt{\sum_{i=1}^{j} V_{X,i}^2}. \tag{15}$$

Assuming implicitly a Log-Normal model for the distribution of the structural resistance, the European EC0 allows evaluating the design value of such quantity through the expression (step (vi) of the procedure):

$$r_d = b g_{rt}(\overline{\mathbf{X}}) \exp\left(-k_{d,\infty}\alpha_{R,t}Q_{R,t} - k_{d,n}\alpha_\Delta Q_\Delta - 0.5Q_R^2\right), \tag{16}$$

where $\bar{r}_t = g_{rt}(\overline{\mathbf{X}})$ is the deterministic value of the resistance when the basic design variables $X_1, X_2, \ldots, X_j$ take their respective mean values; $Q_{R,t} = \sqrt{\ln(V_{R,t}^2 + 1)}$, $Q_\Delta = \sqrt{\ln(V_\Delta^2 + 1)}$ and $Q_R = \sqrt{\ln(V_R^2 + 1)}$ are dimensionless measures of the statistical dispersion affecting the random variables r_t, δ and r; $\alpha_{R,t} = Q_{R,t}/Q_R$ and $\alpha_\Delta = Q_\Delta/Q_R$ are dimensionless weight factors, while $k_{d,n}$ is the pertinent design fractile factor for n samples and $k_{d,\infty}$ is its limit as n tends to $+\infty$. To be consistent with the EC0 provisions, it can be assumed $k_{d,n} = 3.64$ for $n = 22$ [10] and $k_{d,\infty} = 3.04$ (which in turn is very close to the fractile factor $k_p = 3.09$ for a Gaussian random variable and a probability of non-exceedance $p = 0.001$).

5.3. Use within structural design

Eq. (16) was applied for different values of the structural slenderness $\lambda = H/t$, that is $\lambda = 2, 5, 7, 10, 15, 20, 25, 30, 35$ and assuming $e = t/6$ as design value of the load eccentricity and $V_{X,1} = 0.127$ and $V_{X,2} = 0.135$ as CoVs for the basic design variables $X_1 = f_c$ (material randomness) and $X_2 = e/t$ (geometrical uncertainty), respectively. The nine data points $\{\lambda_i, \tilde{r}_{d,i}\}$ so obtained (Fig. 11, Crosses) have been approximated with the following best-fit quadratic expression:

$$\tilde{r}_d = \frac{1}{2}\left[\frac{10}{e} - \frac{\lambda}{100e} - 4 \times 10^{-4}\lambda^2\right], \tag{17}$$

where $\tilde{r}_{d,i} = r_{d,i}/(f_c L t)$ is the normalised structural capacity of the panel.

Fig. 11 illustrates the resulting curve (thick dashed line), which clearly gives a more representative and less conservative prediction of actual panel capacity for slender panels when compared to those derived using existing design techniques, though still provides an adequate margin of safety. By way of example, for a panel of slenderness $\lambda = 30$ one can derive a normalised design value of $N_u/bf_c t = 0.141$(Fig. 11). Taking $\phi = 1$ and substituting the appropriate values for panels tested as part of this study, a design axial capacity of 254 kN is obtained. While this figure is still much lower than those observed in testing (Table 2), it is more suitable than the alternative code-compliant designs, all of which would predict a design capacity of zero. Importantly, partial safety for both materials and actions should be applied in a practical design situation.

A sensitivity study was also undertaken to investigate the influence of reducing the number of experimental data points available to the design engineer. As such further analyses were performed using the top or bottom 50% of panel test capacities at each value of slenderness (best and worst cases). The resulting boundaries (thin solid lines) are also illustrated on Fig. 11, and appear to be very close to the proposed resistance curve. This therefore demonstrates the robustness of the proposed approach against the number of samples available for the application of the DAT procedure.

6. Conclusions and recommendations

The appropriateness of existing design methods for pre-cast slender RC panels has been assessed. The experimental investigations demonstrate a significant conservatism when designing slender pre-cast RC wall panels to current design codes. This results from the inability of the simplified analytical models to account for the true non-linear behaviour when such an element is subjected to an eccentric axial load.

The research has demonstrated the potential of a semi-empirical semi-probabilistic DAT (Design Assisted by Testing) methodology, enabled within the European design code, to derive more representative design values. In order to use this procedure, an alternative resistance function has been devised, utilising a lumped-plasticity computational model with a non-linear fibre hinge at the position of the panel's critical section. This approach was shown to effectively represent the structural response of slender RC panels, with a very good correlation between numerical and experimental values of the structural resistance. Further, this agreement was achieved using a relatively simple computational model, with all analysis run on a standard, consumer-grade laptop. The proposed design method is therefore suitable, provided that it incorporates the statistical analysis required by the DAT procedure.

The design curve so obtained shows an increased structural capacity for slender elements, which better reflects the experimental data and can therefore result in more structurally efficient RC panels. Moreover, the fibre-hinge modelling potentially provides engineers with an effective design tool, which is also easily adaptable to situations with non-standard concrete mixes.

Acknowledgments

This study has been developed as part of the first author's EngD (Engineering Doctorate) project, co-sponsored by the ESPRC (the UK Engineering and Physical Sciences Research Council) and Hanson Structherm, whose financial support is gratefully acknowledged.

Appendix A. Static equilibrium and free body analysis at panel failure

By way of example, let us consider the simply-supported RC panel with $H = 3000$ mm and $e = t/6 = 16.7$ mm, corresponding to the thick dashed curve in Fig. 7, where the ultimate values of axial force and transverse displacement are $N_U = 531$ kN (resistance value at failure) and $\delta' = 9.0$ mm, respectively. Looking now at the stress distribution along the depth of the critical section, depicted within Fig. 5(c), one can observe that the central steel reinforcement is in tension at failure, being $F_{steel} = 17$ kN. It follows that the resultant concrete force at failure is $F_c = N_U - (-F_{steel}) = 548$ kN, which is proportional to the area of the concrete stress diagram shown in Fig. 5(c), that is:

$$F_c = \sum_i \sigma_{c,i} A_{c,i} = 548 \text{ kN}, \tag{A.1}$$

where $A_{c,i}$ is the area of the ith concrete fibre considered in the model, $\sigma_{c,i}$ is the corresponding stress given by the non-linear static analysis and the summation involves all the fibres in compression. The centroid of the stress diagram also allows the determination of the exact position, where the resultant concrete force is applied:

$$\bar{y} = \frac{1}{F_c} \sum_i \sigma_{c,i} A_{c,i} y_i = 24.78 \text{ mm}, \tag{A.2}$$

as illustrated in Fig. 5(c), and since the steel reinforcement is centrally placed, the internal moment at failure is given by:

$$M_{int} = F_c \bar{y} = 13.58 \text{ kNm}. \tag{A.3}$$

To take into account the effects of any accidental eccentricity that may affect the stability of the panel, a notional horizontal force F_{NH} has been also applied at mid-span (see Fig. 5(a)), whose magnitude is assumed to be proportional to the sought ultimate axial capacity:

$$F_{NH} = \psi N_U, \tag{A.3}$$

where

$$\psi = \max\left\{\frac{1}{100}, \frac{t/3}{H}\right\} = 0.0111. \tag{A.4}$$

If we now consider the global equilibrium of the panel, the horizontal reactions forces R_1 (at top support) and R_2 (at the base) must be 0.03 kN and 5.87 kN respectively.

Finally, if we examine the free body diagram of the top part of the panel, also included as part of Fig. 5(a), the externally applied moment at the point of buckling failure (M) can be evaluated as (taking moments about the central steel fibre at mid-span position, i.e. point A within Fig. 5(c)):

$$M = N_U(e + \delta') + R_1 \frac{H}{2} = 531 \times (0.0167 + 0.0090) - (0.03 \times 1.5) = 13.58 \text{ kNm} \tag{A.5}$$

This is (as expected) equal to the corresponding value derived as part of Eq. (A.3), which is dictated by the moment rotation plot included as part of Fig. 5(d), and which was generated by consideration of the structural cross section and appropriate material models.

References

[1] American Concrete Institute, ACI 318-05. Building code requirements for structural concrete and commentary. Farmington Hills; 2005.
[2] Standard Association of Australia, AS 3600-2009, Concrete structures amendment 1-2010. Sydney; 2010.
[3] Comité Européen de Normalisation, EN 1992-1-1. Eurocode 2 design of concrete structures Part 1–1 General rules and rules for buildings. Brussels; 2004.
[4] Wight JK, Macgregor JG. Reinforced concrete mechanics and design. 5th ed. San Jose: Pearson Education International; 2009.
[5] De Falco A, Lucchesi M. Stability of columns with no tension strength and bounded compressive strength and deformability. Int J Solids Struct 2002;39(25):6191–210.
[6] Doh JH, Fragomeni S. Evaluation of experimental work on concrete walls in one-way and two-way action. Aust J Struct Eng 2005;6(1):103–15.
[7] Fragomeni S, Mendis AM, Grayson WR. Review of reinforced concrete wall design formulas. ACI Struct J 1994;91(5):521–9.
[8] Crozier DA, Sanjayan JG. Slender reinforced concrete panel research. In: Proceedings of 18th Biennial conference on, concrete; 1997. p. 347–53.
[9] Robinson GP, Palmeri A, Austin SA. Tension softening effects on the buckling behaviour of slender concrete wall panels. In: Proceedings of ISEC-6 on modern methods and advances in structural engineering and, construction; 2011. p. 715–20.
[10] Comité Européen de Normalisation, EN 1990. Eurocode 0 basis of structural design. Brussels; 2002.
[11] Gulvanessian M, Calgaro JA, Holicky M. Designer's guide to EN1990 Eurocode: basis of structural design. London: Thomas Telford Publishing; 2002.
[12] Robinson GP, Palmeri A, Austin SA. Implications of EC2 on the design of simply supported precast RC panels under eccentric axial load. In: Proceedings of fib symposium on concrete engineering for excellence and efficiency; 2011. p. 123–7.
[13] Doh JH, Fragomeni S, Loo YC. Strength tests on slender reinforced concrete walls in one and two way action. In: Proceedings of EASEC8 on structural engineering and, construction; 2001. p. 1302.
[14] Kripanarayanan KM. Interesting aspects of the empirical wall design equation. ACI Struct J 1977;74(5):204–7.
[15] Pillai SU, Parthasarathy CV. Ultimate strength and design of concrete walls. J Build Environ 1977;12(1):25–9.
[16] Sanjayan JG, Crozier DA, Cheuk JG. Tension softening effects on the buckling behaviour of slender concrete wall panels. In: Proceeding of 5th international conference on concrete, engineering and technology; 1997. p. 132–49.
[17] Monti G, Alessandri S, Santini S. Design by testing: a procedure for the statistical determination of capacity models. J Constr Build Mater 2009;23(2009):1487–94.
[18] Dubina D. Structural analysis and design by testing of cold-formed steel structures. J Thin Wall Struct 2008;46(2008):741–64.
[19] CSI SAP 2000 v-14, Integrated finite element and design of structures analysis reference manual. Berkley: Computers and Structures Inc.; 2010.
[20] Inel M, Ozmen HB. Effects of plastic hinge properties in nonlinear analysis of reinforced concrete buildings. J Eng Struct 2006;28(2006):1494–502.
[21] Tsai WT. Uniaxial compression stress–strain relation of concrete. J Struct Eng 1988;114(9):2133–6.
[22] Panagiotakos TB, Fardis MN. Deformations of reinforced concrete members at yielding and ultimate. ACI Struct J 2001;98(2):135–48.

[23] Mander JB, Priestley MJN, Park R. Theoretical stress–strain model of confined concrete. J Struct Eng 1988;114(8):1804–26.
[24] Kent DC, Park R. Flexural members with confined concrete. J Struct Div ASCE 1971;97(ST7):1969–90.
[25] Scott BD, Park R, Priestly MJN. Stress–strain behaviour of concrete confined by overlapping hoops at low and high strain rates. J Am Concr Inst 1982;79:13–27.
[26] Bamforth P, Chisholm D, Gibbs J, Harrison T. Properties of concrete for use in Eurocode 2. 1st ed. Surrey: The Concrete Centre; 2008.
[27] Gilbert RI. Time effects in concrete structures. 1st ed. Amsterdam: Elsevier Science; 1988.